Research on the long-term performance degradation mechanism of anti-corrosion coatings on metal surfaces under marine climate conditions

Noam W. Buckley[1]

[1]University of Miami

***Corresponding Author:**
noamwbuckley@gmail.com

Received: 09/10/2024
Revised: 29/12/2024
Accepted: 16/01/2025
Published: 28/02/2025

Abstract: This study explores the development of a durable anti-corrosion coating for marine environments by chemically modifying water-based polyurethane (PU) with organosilicon. Polydimethylsiloxane (PDMS) was used as a functional monomer, reacting with methyl diisocyanate (MDI), polyethylene glycol 1000 (PEG1000), and dimethylolpropionic acid (DMPA) to synthesize an organosilicon-modified PU (SiPU) emulsion. The SiPU exhibited an initial decomposition temperature of 331 °C—91 °C higher than unmodified PU—and a slightly lower glass transition temperature (−32.8 ŕC), indicating improved thermal flexibility. Coatings prepared with PDMS-g-PA composites showed significantly higher impedance and larger Nyquist arcs after 35 days in 0.1 mol/L HCl. The 5% PDMS coating (P-5) achieved the highest adhesion grade (5A) and showed a 35.08% increase in bond strength. Under varying chloride conditions, P-5 maintained a stable open-circuit potential and lower corrosion current density over 30 days, confirming enhanced adhesion, thermal stability, and corrosion resistance.

Keywords: marine climate, organosilicon-modified polyurethane, corrosion-resistant coating, long-term performance, metal corrosion protection

1 | Introduction

In the vast and boundless marine world, marine engineering plays a crucial role [1]. From offshore oil drilling platforms to cross-sea bridges, from undersea tunnels to marine vessels, these marine engineering facilities play an irreplaceable role in driving economic development, promoting communication, and ensuring national security [2, 3, 4]. However, the marine environment is extremely harsh, characterized by high humidity, high salinity, and strong corrosion, posing severe challenges to marine engineering facilities, with corrosion issues being particularly prominent [5, 6, 7]. Marine corrosion refers to the electrochemical and chemical corrosion of metallic materials in marine environments [8, 9]. Seawater is a complex electrolyte solution containing large amounts of chloride ions, sodium ions, magnesium ions, and other ions, which accelerate metal corrosion [10, 11]. Additionally, factors such as marine biofouling, wave impact, and temperature fluctuations can exacerbate corrosion severity [12]. Corrosion not only reduces the structural strength and service life of marine engineering facilities but may also lead to severe safety incidents and environmental pollution. The application

of corrosion-resistant coatings on metal surfaces has become a critical method for ensuring the safety of marine engineering facilities [13, 14, 15, 16].

Coating protection is a widely used corrosion prevention method [17]. By applying a layer of coating with excellent corrosion resistance to the metal surface, the contact between seawater and metal can be effectively blocked, thereby slowing down the corrosion process [18, 19, 20]. Common coating materials include epoxy resin, polyurethane, and fluorocarbon coatings [21]. These coatings have good adhesion, water resistance, and chemical corrosion resistance [22]. However, coatings are susceptible to wear, scratches, and aging in long-term marine environments, which can reduce their protective effectiveness [23, 24]. Therefore, studying the long-term performance degradation mechanisms of corrosion-resistant coatings on metal surfaces, conducting regular inspections and maintenance of coatings, and promptly identifying and repairing damaged areas are crucial for ensuring the safe operation and sustainable development of marine engineering projects [25, 26, 27, 28].

Liang, Shi and Li [29] emphasizes the importance of effective protective and corrosion-resistant technologies for ensuring the safety and usability of marine facilities, and based on a literature review, analyzes the challenges currently faced by marine anti-fouling and corrosion-resistant coating technologies and provides recommendations. Xue, Liang and Zhang [30] prepared a superhydrophobic silane-modified montmorillonite/epoxy (SM-MMT/EP) coating. Experimental evaluations of its wettability, corrosion resistance, and other properties demonstrated that the superhydrophobic SM-MMT/EP coating exhibits excellent overall performance and superior corrosion resistance in marine environments. Sabet-Bokati et al. [31] investigated the long-term effectiveness of sustainable anti-corrosion coatings in static and dynamic humid environments, aiming to simulate typical conditions in marine environments, and reiterated the importance of selecting inhibitors suitable for specific environmental conditions. Wang et al. [32] indicated that corrosion is a common issue in marine facilities and proposed a bibliometric analysis of relevant research in this field using bibliometric and information visualization analysis methods, pointing out that research in the field of marine environment corrosion is generally showing a growing trend. Vera et al. [33] evaluated the performance of three coating systems in marine environments, noting that these systems exhibit good adhesion and resistance to delamination, with differences observed between primer and topcoat applications. Song and Feng [34] discusses research on coating microstructure and corrosion resistance, examining the influence of substrate effects and environmental factors on coating protective capabilities, and emphasizes that defects in organic coatings are a significant cause of corrosion damage. Wu et al. [35] identifies microcrack damage repair and microbial contamination prevention as the primary challenges for corrosion-resistant coatings on underwater facility surfaces. It combines water-triggered self-healing microcapsules with low-surface-energy fluoropolymers to prepare corrosion-resistant coatings with underwater self-healing and biofouling protection properties, verifying that the coating exhibits good mechanical and environmental stability. Yu et al. [36] conducted research on the corrosion resistance of organic coatings used in marine engineering under simulated Arctic offshore environmental conditions, providing references for selecting appropriate corrosion-resistant coatings in polar environments. Zhao et al. [37] noted that defects in steel surface protective coating systems are a common phenomenon in engineering applications. Based on this, a composite coating system was adopted to protect carbon steel from corrosion in marine environments, and experiments revealed the effectiveness of this system. Zhang et al. [38] used the cold spraying method to manufacture a polyvinyl alcohol-polyvinylidene fluoride-fluorocarbon polymer (PPFMC) multi-level rough superhydrophobic coating, which effectively improved the corrosion resistance and anti-icing performance of aluminum alloys, while also exhibiting stability and drag-reducing properties. Eom, Kim and Lee [39] evaluated coating systems for preventing corrosion in offshore wind power plants and the adhesion strength of each coating system. The results indicated that adhesion strength varies with exposure

time, and the degradation of adhesion strength is related to the fracture type of each coating. Wang et al. [40] experimentally simulated the corrosion mechanism and rate of aluminum-zinc coatings in marine environments and investigated the role of aluminum, which has been less studied in previous literature.

Silicone resins are renowned for their excellent high and low temperature resistance, hydrophobicity, weather resistance, and chemical inertness. This study focuses on modifying water-based polyurethane (PU) resins through silicone chemistry, aiming to combine the environmental friendliness and good film-forming properties of water-based PU with the outstanding weather resistance of silicone to develop a new type of high-performance, environmentally friendly anti-corrosion coating suitable for marine climate conditions. Hydroxypropyl polysiloxane (PDMS) was selected as the functionalized hydroxy monomer and reacted with main raw materials such as diphenylmethane diisocyanate (MDI) and polyethylene glycol (PEG1000); Dihydroxymethylpropionic acid (DMPA) was used as a hydrophilic chain extender. Through molecular design, silicone segments were introduced into the polyurethane main chain or side chains to synthesize silicone-modified water-based polyurethane (SiPU) emulsion. It is anticipated that the introduction of PDMS will significantly improve the hydrophobicity, thermal stability, hydrolytic resistance, and corrosion resistance of pure PU coatings. The study will systematically investigate the effects of organosilicon content and synthesis process parameters on SiPU emulsion stability, coating microstructure (characterized by FT-IR, XRD, SEM/EDS, XPS), , thermal properties (via DSC and TG analysis), basic physical and mechanical properties (adhesion, hardness, flexibility), and key corrosion-resistant electrochemical properties (via electrochemical impedance spectroscopy (EIS) and Tafel polarization curves, evaluated in simulated marine environments using NaCl solutions and acidic/alkaline media). Furthermore, to explore its application potential in real-world scenarios, the optimized SiPU resin is combined with functional monomers such as acrylic esters (e.g., BA, MMA, St) via radical polymerization to prepare organosilicon composite resins (PDMS-g-PA), which are then coated onto steel substrate materials, Systematically studying its long-term adhesion evolution (tape peel test, adhesive strength test) and electrochemical corrosion protection behavior (long-term open-circuit potential monitoring, polarization curve analysis) under simulated marine climate conditions (different Cl^- concentrations, carbonization conditions) to elucidate the mechanisms underlying its long-term performance degradation.

2 | Preparation and characterization of organosilicon-modified water-based polyurethane emulsion

Metal materials are widely used in various fields due to their excellent mechanical and process properties. However, metal corrosion significantly shortens the service life of metal materials, resulting in substantial economic losses. To slow down metal corrosion, coatings can be applied to the metal surface as a barrier. Among these, anti-corrosion coatings can effectively isolate corrosive liquids to slow down the corrosion rate of aluminum alloys. This paper primarily investigates the synthesis and coating performance of organosilicon-modified water-based polyurethane emulsions under marine climatic conditions.

Organosilicon, also known as polysiloxane. The preparation of high-corrosion-resistant water-based resins in this chapter primarily uses hydroxypropyl polysiloxane (PDMS), diphenylmethane diisocyanate, and polyethylene glycol 1000 as main raw materials. The organosilicon hydroxypropyl polysiloxane serves as the monomer providing functionalized hydroxyl groups, enabling it to react with isocyanate groups. Dihydroxymethylpropionic acid is used as a hydrophilic chain extender to synthesize organosilicon-modified

water-based polyurethane emulsions and coatings with excellent compatibility and water resistance. FT-IR, DSC, and TG tests are conducted to analyze the structure and compatibility of the samples. Tests on film-forming properties, coating water resistance, and coating water absorption rate are performed to investigate the impact of different synthesis factors and variables on the comprehensive performance of the product, and to determine the optimal synthesis process.

2.1 | Main reagents and instruments

The main reagents and instruments used in the experiment are shown in Tables 1 and 2, respectively.

TABLE 1 Reagents

Reagent names	Specification	Manufacturer
Di-phenylmethane diisocyanate (MDI)	Industrial grade	BASF
Polyethylene glycol (PEG1000)	Analysis of purity	Sinopharm Chemical Reagent Co., Ltd.
Dimethylolpropionic acid (DMPA)	Industrial grade	Evonik Degussa
Hydroxypropyl polydimethylsiloxane (PDMS)	Chemical purity,$\bar{M}_n = 1000$	Shanghai Sili Industry & Trade Co., Ltd.
Dibutyltin dilaurate (DBTDL)	Analysis of purity	China National Pharmaceutical Group Chemical Reagent Co., Ltd.
Triethylamine (TEA)	Analysis of purity	China National Pharmaceutical Group Chemical Reagent Co., Ltd.

TABLE 2 Instruments

Instrument Name	Manufacturer
Digital display constant temperature water bath	Shanghai Meixiang Instrument Co., Ltd.
Electric stirrer	Jintan Huanyu Scientific Instrument Factory
Constant temperature drying oven	Shanghai Heng Technology Co., Ltd.
Electronic balance	OHAUS
Fourier infrared spectrometer Spectrum 100	Perkin-Elmer
Differential scanning calorimeter DSC 821	Mettler
Thermogravimetric analyzer TG 209 F3	Hitachi

2.2 | Structural characterization and performance testing

2.2.1 | Test characterization

1) Use a contact angle tester (Harke-SPCA) to measure the contact angle (WCA) and rolling angle (SA) of the sample. The droplet volume for contact angle testing is 6 μL, and the droplet volume for rolling angle testing is 12 μL. Each sample is tested five times at different positions, and the average value is taken.

2) Use a video optical contact angle meter (OCA25) to capture images of the droplet rolling and adhering on the sample surface. The droplet volume is 12 μL.

3) Tape tests are conducted on the samples. The samples are placed on a horizontal smooth surface, and a

2.5M transparent tape is gently applied to cover the sample surface. A weight is rolled back and forth three times on the tape, after which the tape is removed. This constitutes one tape test, and the procedure can be repeated multiple times.

4) After gold coating the sample, observe its morphology using a scanning electron microscope (SEM, JSM-6510LV) at a voltage of 5 kV.

5) An energy-dispersive spectrometer (EDS) was used to determine the elemental distribution and composition at 10 kV.

6) The chemical composition of the sample surface was analyzed using X-ray photoelectron spectroscopy (XPS, Escalab 250Xi) under a monochromatic Al-focused X-ray source (1506.4 eV). The spectral data obtained were analyzed and fitted using Avantage software.

7) The infrared spectrum of the sample surface was collected and analyzed using attenuated total reflection Fourier transform infrared spectroscopy (ATR-FTIR, Nicolet 6500), with a scanning range of 5000–500 cm^{-1}.

8) Tafel polarization curves (CHI 660A) were measured on an electrochemical workstation using a three-electrode system (the test sample as the working electrode, platinum sheet and saturated calomel electrode as the counter electrode and reference electrode, respectively) at a scanning rate of 2 mV/s within the voltage range of ±280 mV vs. OCP. The corrosion resistance of the sample in Cl^-, acidic, and alkaline environments was tested in 3.7 wt.% NaCl aqueous solution, pH = 2.8 HCl solution, and pH = 11 $NH_3 \cdot H_2O$ solution to evaluate the sample's corrosion resistance in Cl^-, acidic, and alkaline environments.

9) Electrochemical impedance spectroscopy (EIS, Solartron Analytical EchemLab XM) was conducted in 3.7 wt.% NaCl solution, the tests were conducted at open-circuit potential within the frequency range of 10^5 Hz to 10^{-3} Hz, with an operating potential amplitude of 12 mV. The test area of the sample was approximately 1 cm^2 in all tests, with the remaining surface covered by insulating tape. Prior to testing, the sample was immersed in the electrolyte solution until the system reached a stable open-circuit potential.

2.2.2 | Rheological testing

Add a drop of the solution to the bottom plate of the rheometer, adjust the distance between the top and bottom plates to 1.5 mm, and select an angular frequency ω of 1 rad/s and a strain γ between 0.1% and 100% to measure the amplitude viscosity. This will help you find the linear viscoelastic region (the range where you can do the test without messing up the sample structure), and then you can scan the frequency to check out the rheological properties of the polymer solution. During the reaction monitoring period, the elastic modulus G' and loss modulus G'' values are obtained every 10 seconds. The angular frequency scan test range is set to 0.01 to 1000 rad/s, γ is 0.1%, and T is 26°C.

2.2.3 | Basic performance testing of coatings

Adhesion test. Adhesion of the coating is tested using a scratch test. Using this tool, the paint film is cut horizontally and vertically at a 90° angle on the prepared coating to form a good lattice pattern. Then, adhesive tape is used to test the coating's peelability. According to ISO 2409 standards, the adhesion grade of the coating is classified from best to worst based on the number of lattice peels, ranging from 0 to 5.

Hardness test. The pencil scratch method is used to test the hardness of the coating. A 700g coating hardness tester is used to determine different hardness grades (from hard to soft, ranging from 9H to 9B) based on

whether the pencil scratches the coating.

Flexibility test. The flexibility of the coating is determined by bending the coating sample around shafts of different diameters. The smallest shaft diameter that does not damage the coating after bending is used as the indicator. Under conditions that do not damage the coating layer, the smaller the shaft diameter, the better the flexibility of the coating.

Transparency test. The transparency of the coating is tested using a UV-visible spectrophotometer. By comparing with uncoated glass, the transparency of coatings with different silicone content can be measured at different wavelengths.

2.2.4 | Shear test

Test the shear strength of the coating using a texture analyzer. Apply the sample evenly to two 2.4 cm × 1.3 cm metal or glass substrates. After the sample has completely cured, perform a coating shear test on the texture analyzer by stretching it.

3 | Study on the coating performance of organosilicon-modified water-based composite resins

The above-mentioned experimental setup for the systematic preparation and structural characterization of organosilicon-modified water-based polyurethane (SiPU) emulsions. This chapter analyzes the results of the coating performance testing experiments.

3.1 | Characterization and test result analysis of organosilicon-modified water-based coatings

3.1.1 | Infrared characterization

The high corrosion-resistant water-based resin SiPU emulsion was first dried at room temperature for 24 hours, then dried in an oven for 24 hours, followed by drying in a vacuum oven for 48 hours. It was then mixed with potassium bromide (KBr), ground uniformly, pressed into tablets, and characterized using a Fourier transform infrared spectrometer (FTIR).

Infrared spectroscopy was used to characterize the structure of the prepared SiPU coating. The infrared spectrum of the organosilicon-modified polyurethane (SiPU) film is shown in Figure 1.

As shown in the figure, 3222 cm^{-1} corresponds to the N-H stretching vibration peak, 1322 cm^{-1} to the N-H bending vibration peak, 1663 cm^{-1} to the C=O hydroxyl stretching vibration peak, 1184 cm^{-1} to the C-N stretching vibration peak, 662 cm^{-1} is the C-H bending vibration peak in the benzene ring, all of which are characteristic absorption peaks of polyurethane; while 1010 cm^{-1} is the Si-O-Si bending vibration absorption peak, and the characteristic absorption peak of -NCO at 2400 cm^{-1} to 2000 cm^{-1} has basically disappeared, indicating that there is no remaining -NCO in the system. From the above, it can be inferred that polyurethane has been formed, and the organosilicon has been incorporated into the polyurethane according to the theoretically designed reaction mechanism.

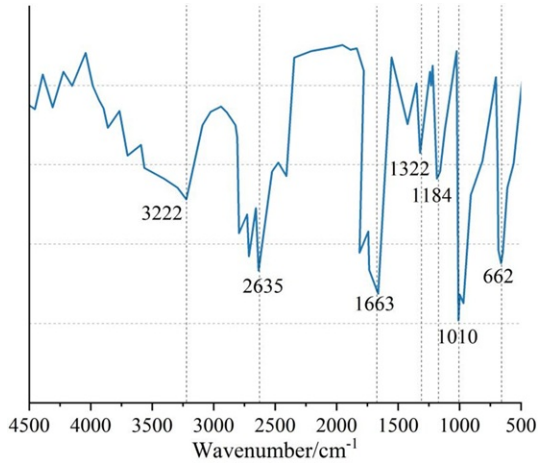

FIGURE 1 Infrared spectrum of organosilicon-modified polyurethane (SiPU) film

3.1.2 | Thermal performance testing

The high corrosion-resistant water-based resin SiPU emulsion was dried at room humidity for 24 hours, then placed in an oven at 60°C for 12 hours, and tested using a thermogravimetric analyzer (TG) at a temperature range of 20–600°C and a testing rate of 20°C/min. The prepared high-corrosion-resistant water-based resin SiPU emulsion was dried at room temperature for 24 hours, then placed in an oven at 60°C for 12 hours, and tested using a differential scanning calorimeter (DSC) with a temperature range of 20–250°C and a heating rate of 10°C/min.

Figures 2 and 3 show the curves obtained from thermal gravimetric analysis (TG) and differential scanning calorimetry (DSC), respectively. The thermodynamic behavior of the coating was analyzed using the TG and DSC curves.

As shown in the curve in Figure 2, the onset point of thermal weight loss for organosilicon-modified water-based PU is higher than the onset decomposition temperature of unmodified conventional PU. The decomposition temperature of SiPU is 331°C, while that of PU is approximately 240°C. Additionally, as indicated by the DTG curve, both the modified and unmodified PU exhibit four decomposition stages; however, the decomposition of organosilicon-modified water-based SiPU is clearly superior. It can be concluded that the introduction of high-temperature-resistant silicon enhances the thermal stability of silicon-containing PU, thereby improving the heat resistance of organosilicon-modified water-based polyurethane.

As shown in Figure 3, the organosilicon-modified water-based PU has only one glass transition temperature (Tg) of -32.8°C, which is slightly lower than that of the unmodified general polyurethane. The unmodified PU has two transition temperatures, namely -30.4°C and -12°C. This indicates that the low-temperature resistance of the organosilicon-modified water-based PU system has been improved compared to the unmodified version, effectively preventing the phenomenon of thermal adhesion and cold brittleness, thereby meeting the project's requirements for high and low temperature resistance, and essentially achieving the purpose of modification.

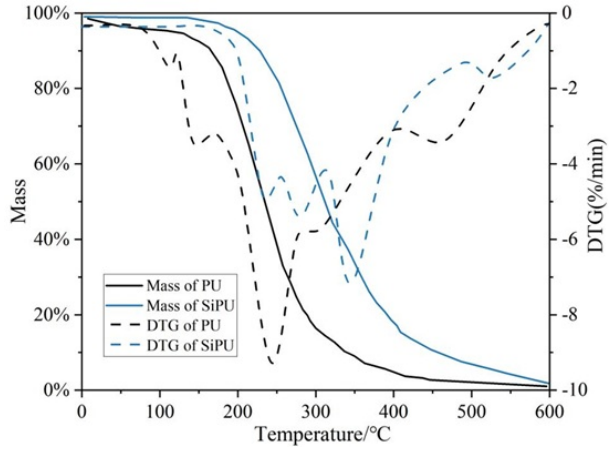

FIGURE 2 TG diagrams of PU and SiPU coatings

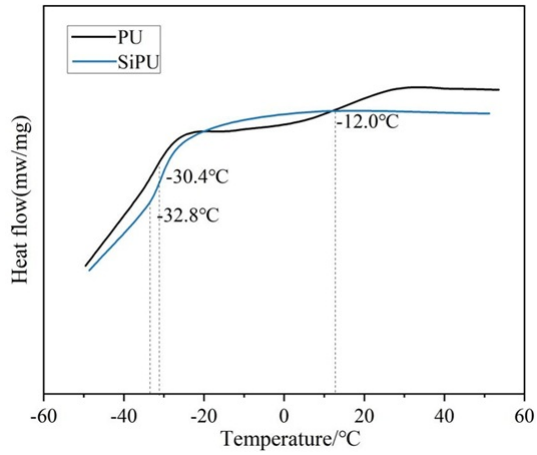

FIGURE 3 DSC diagrams of PU and SiPU coatings

3.2 | Study on the performance of organosilicon composite resins

The characterization tests of the organosilicon-modified water-based polyurethane emulsion described above were completed, validating the effectiveness of the modified water-based polyurethane SiPU. Next, performance testing and research were conducted on the organosilicon composite resin of this material.

Through efficient radical polymerization reactions, various functional acrylic ester monomers (BA, MMA, St, etc.) were used as the polymer matrix to enhance substrate adhesion, and vinyl-functionalized organosilicon prepolymers (PDMS) were added to modify the surface properties of the coating.

PDMS was synthesized using an ring-opening polymerization method. The organosilicon composite resin PDMS-g-PA was prepared using a radical polymerization method.

3.2.1 | Rheological analysis of organosilicon composite resins

To thoroughly investigate the viscoelastic behavior of the materials under study, a comprehensive series of rheological tests was carried out on the various polymer solutions. These experiments were designed to quantitatively assess both the elastic and viscous characteristics of the polymers. Specifically, the storage modulus (G'), which serves as an indicator of the material's elastic or energy-storing response, and the loss modulus (G''), which represents the viscous or energy-dissipating behavior, were measured across a range of conditions. By analyzing these parameters, a deeper understanding of the polymers' deformation and flow characteristics can be achieved. The resulting rheological curves for the PA, PDMS, and PDMS-g-PA polymer samples, which clearly illustrate their viscoelastic properties and highlight differences in elasticity and viscosity, are presented in Figures 4 through 6, respectively. These figures provide valuable insight into the molecular structure and dynamic response of each polymer system, offering a basis for comparison and further material optimization.

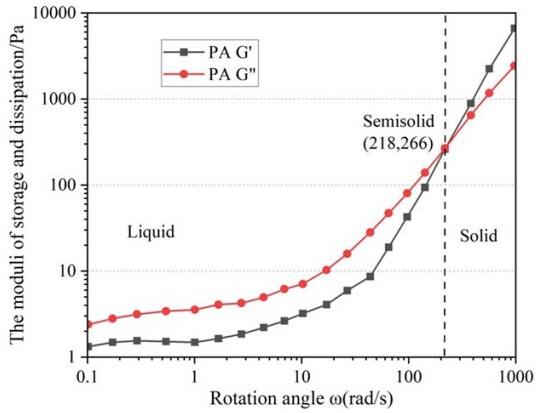

FIGURE 4 The rheological curve of PA

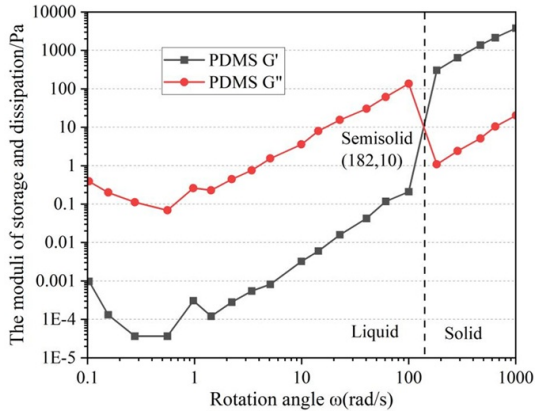

FIGURE 5 The rheological curve of PDMS

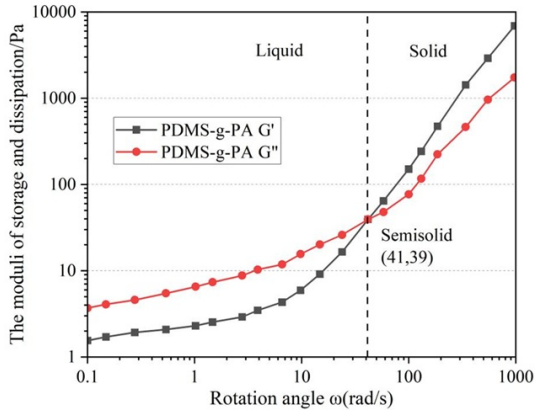

FIGURE 6 The rheological curve of PDMS-g-PA

As can be clearly seen from the Figure above, the patterns of the three polymers are consistent. At low frequencies, the loss modulus G" is greater than the storage modulus G', and viscosity dominates, causing the material to exhibit liquid-like behavior; At high frequencies, the storage modulus G' is greater than the loss modulus G", and elasticity dominates, causing the material to exhibit solid-like properties; there is also a point where the storage modulus G' equals the loss modulus G", resulting in a semi-solid state with gel-like properties. This is a typical characteristic of non-crosslinked polymers and aligns with the results of the experimentally designed linear polymers.

For non-crosslinked polymers, the magnitude of the angular frequency at the intersection of G' and G" in the rheological curve can roughly indicate the average molar mass of the polymer; the larger the angular frequency ω, the smaller the average molar mass M. As shown in Figures 4 to 6, the angular frequencies corresponding to the intersection points for PA, PDMS, and PDMS-g-PA polymers are 218 rad/s, 182 rad/s, and 41 rad/s, respectively. Therefore, from this perspective, it can be inferred that M(PA) < M(PDMS) < M(PDMS-g-PA).

3.2.2 | Crystal structure analysis of organosilicon composite resin

The crystallization behavior of polymers was determined through X-ray diffraction analysis, and the effect of introducing organosilicon on the crystalline structure of polyacrylate materials was investigated. Figures 7 and 8 show the XRD spectra for different PDMS contents. Figure 7 shows the XRD spectrum for 2θ = 0–10°, and Figure 8 shows the spectrum for 2θ = 10–100°.

As shown in the figure, the four polymers—PA, 5% PDMS-g-PA, 10% PDMS-g-PA, and 15% PDMS-g-PA—all exhibit a broad diffuse peak at 2θ = 2°, along with three sharp peaks between 60° and 75°. This indicates that the crystalline structure of the polyacrylate films grafted with different concentrations of PDMS remains unchanged. The introduction of silicone does not disrupt the aggregated state of the acrylate structure, which may suggest the presence of microphase separation behavior within the copolymer matrix.

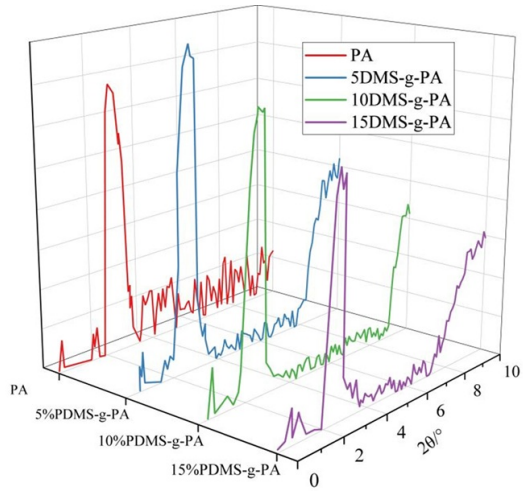

FIGURE 7 XRD spectra of different PDMS contents(2θ=0-10°)

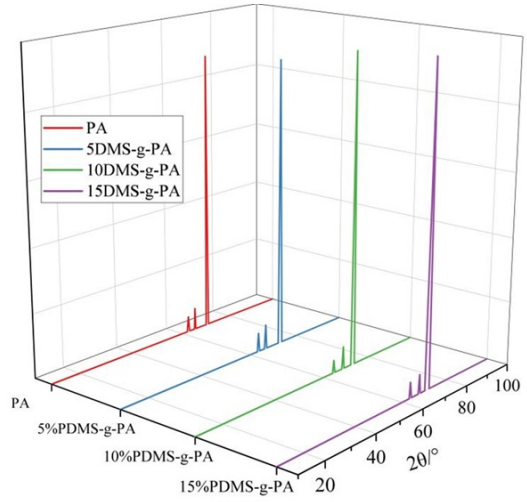

FIGURE 8 XRD spectra of different PDMS contents(2θ=10-100°)

3.2.3 | Thermal performance analysis of organic silicon composite resins

The thermal stability of PA and PDMS-g-PA films was tested using TGA. The TGA curves of PA and PDMS-g-PA polymers are shown in Figure 9.

As shown in Figure 9, polyacrylate film decomposes at 442.37°C. For block copolymer organosilicon composite resin, there are two decomposition stages: the first decomposition stage occurs at 404.28°C, which is attributed to the decomposition of the acrylate polymer segments, and the second decomposition stage occurs at 567.40°C, primarily due to the decomposition of the organosilicon component. The higher decomposition temperature indicates that the target product, the organosilicon composite resin, possesses excellent thermal

stability and a multi-phase structure.

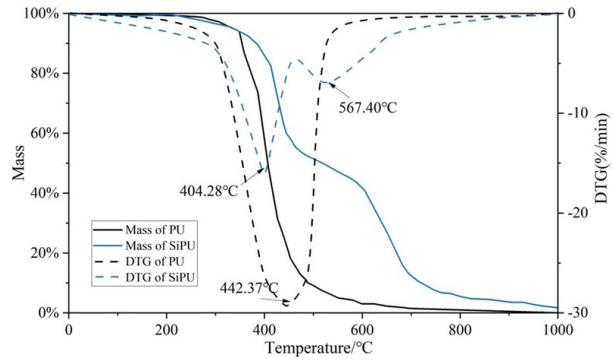

FIGURE 9 TGA curves of PA and PDMS-g-PA polymers

3.2.4 | Electrochemical analysis of coatings

To assess coating corrosion rates, electrochemical impedance spectroscopy (EIS) tests were performed on composite coatings. Figures 10 and 11 display the Bode plots for PA, 5% PDMS-g-PA, 10% PDMS-g-PA, and 15% PDMS-g-PA coatings (on metal substrates) after immersion in 0.1 mol/L HCl for 35 days. Figure 12 presents the corresponding Nyquist plots.

The Nyquist plots show that the Z"–Z' impedance curves for all polymer coatings continue to rise, indicating that the coatings remain in a protective state with good corrosion resistance. Moreover, as the PDMS content increases, the impedance arc becomes larger, suggesting that PDMS-g-PA coatings provide enhanced corrosion resistance in acidic environments compared to PA coatings, especially at higher PDMS concentrations.

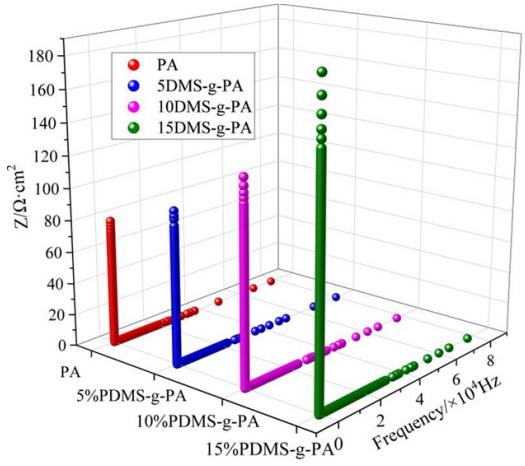

FIGURE 10 Electrochemical impedance diagram of coating acid corrosion(Bode)

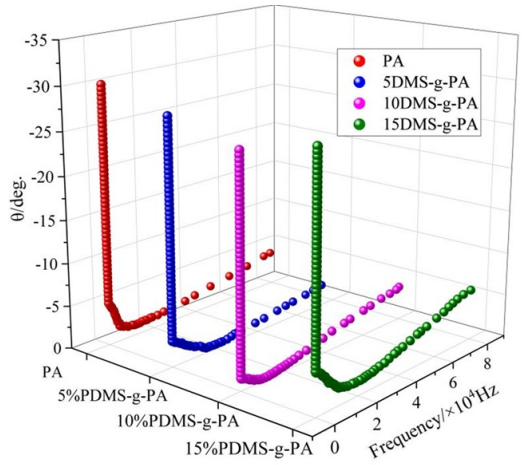

FIGURE 11 Electrochemical impedance diagram of coating acid corrosion(Bode)

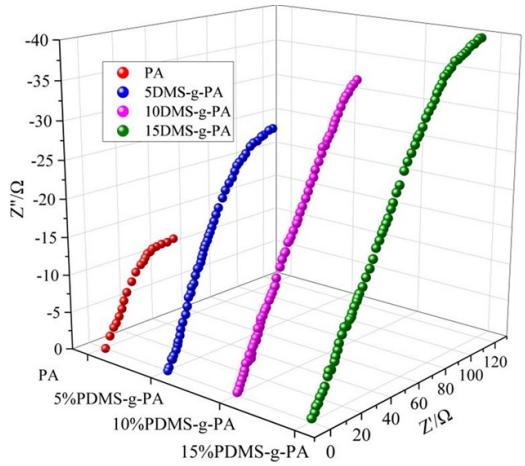

FIGURE 12 Electrochemical impedance diagram of coating acid corrosion(Nyquist)

4 | Research on the long-term corrosion resistance of organic silicon polymer steel sheet coatings

The previous sections on the rheological properties, crystal structure, thermal stability, and short-term electrochemical corrosion protection performance (EIS) of organosilicon composite resins (PDMS-g-PA) indicate that the introduction of PDMS effectively improves the performance of polyacrylate-based coatings and demonstrates superior protective effects compared to pure PA coatings in acidic environments, with impedance increasing as PDMS content increases. However, the excellent performance of the coating in laboratory accelerated testing must be validated in actual or simulated long-term harsh marine service environments to truly assess its potential as a long-term corrosion-resistant coating and its performance degradation patterns.

Therefore, this chapter will focus on applying the optimized silicone-modified composite resin (PDMS-g-PA) to steel substrate materials, systematically investigating its long-term corrosion protection performance, adhesion evolution, and failure mechanisms under simulated marine climate conditions (including varying chloride ion concentrations and carbonation effects).

4.1 | Application of organosilicon coatings on steel sheets in marine climates

The durability of reinforced concrete is largely dependent on environmental conditions such as carbonation, corrosion, alkali-silica reaction, and freeze-thaw cycles. When concrete is exposed to corrosive media, particularly chlorine-containing environments, chloride ions can penetrate into hardened concrete. In this way, once the chloride ion concentration at the steel/concrete interface exceeds the threshold, the passivation layer is destroyed. Several methods are widely used to delay steel corrosion, including the application of corrosion-resistant coatings on reinforcing bars. Organic polymers such as polyurethane, epoxy resin, and acrylic are the most widely used coatings, offering excellent adhesion strength, waterproofing, and corrosion resistance. However, issues such as polymer aging, low permeability, and unreliable durability lead to the need for frequent maintenance or replacement of the coatings.

Organosilicon composite resin polymers are frequently used in the field of reinforcing steel corrosion protection due to their superior performance, such as using geopolymers to replace cement in concrete preparation and geopolymer-based corrosion-resistant coatings. Many researchers have found that geopolymer concrete exhibits better corrosion resistance than ordinary Portland cement concrete. Some studies hypothesize that the LDHs and C(N)-A-S-H phases in slag-based geopolymers possess higher chloride ion binding capacity, which may also contribute to enhanced resistance against chloride ion penetration. The feasibility of using organosilicon polymers as coatings for marine concrete in marine climates was evaluated through field experiments. After six months of exposure in the tidal zone, the geopolymer coatings on coastal concrete surfaces showed no signs of sulfate erosion, demonstrating excellent corrosion resistance. Organosilicon polymer coatings exhibit high bond strength with both cement concrete and steel plates and can significantly increase the resistivity of the substrate. However, pure geopolymers still face the issue of significant shrinkage during service, with microcracks inducing and accelerating the intrusion of corrosive ions, leading to coating failure. This makes drying shrinkage one of the most critical issues to overcome in the application of geopolymers as corrosion-resistant coatings for reinforcing steel. The use of toughened polymers and liquid polymers to modify geopolymers can effectively break through the limitations of geopolymer coating applications. In the preceding text, vinyl-functional organosilicon prepolymers (PDMS) were used at 5%, 10%, and 15% by weight, and three silane coupling agents (SCA) at a 1% loading. The study found that organosilicon-modified water-based polymers exhibit superior performance in terms of shrinkage, adhesion, abrasion resistance, and resistance to chloride ion corrosion, and demonstrate good durability in seawater and carbonation environments. Most researchers have focused on the application of polymer-modified geopolymers in concrete, with few exploring their use as coatings on reinforcing steel surfaces.

The organosilicon-modified water-based composite resin polymer prepared in the previous chapter was applied to steel plates, ensuring the same coating mass per unit area to achieve uniformly thick modified geopolymer coatings. Two different testing methods (tape peel test and pull-off test) were used to investigate the effect of different PDMS content (0%, 5%, 10%, 15%) on polymer adhesion. SEM microstructural characterization was employed to observe the surface morphology of the modified geopolymer coating and the

interfacial bonding between the coating and the steel plate.

Additionally, the two groups of PDMS-modified geopolymer steel sheet coatings with better comprehensive performance (P-5 and P-10) were subjected to long-term corrosion monitoring using an electrochemical workstation. Open-circuit potential (OVP) and polarization curve (TP) tests were conducted on samples immersed in different simulated solutions at 1 day, 3 days, 5 days, 10 days, 20 days, 30 days, and 60 days. The macro-morphology and corrosion rate of the samples after 60 days of immersion were then analyzed in conjunction with the open-circuit potential (OVP) and polarization curve (TP) tests to comprehensively evaluate the corrosion-resistant performance and corrosion inhibition mechanism of the modified polyethylene glycol coatings.

4.2 | Experimental analysis of coating corrosion resistance performance

4.2.1 | Tape peel test

The adhesion of the modified geopolymer coating was qualitatively evaluated using the ASTM tape peel test, and the results are shown in Table 3.

TABLE 3 Adhesion level of geopolymer coating with different PDMS dosages

	P-0	P-5	P-10	P-15
3d	1A	4A	4A	3A
5d	2A	5A	4A	2A
10d	2A	5A	5A	2A
20d	1A	5A	5A	1A
30d	1A	5A	5A	1A

The pure organosilicon polymer coating PA (P-0) exhibited pitting corrosion at the edges after 10 days of curing and small-area rusting after 30 days of curing. This is because the polymer undergoes significant drying shrinkage, and the stress generated by shrinkage easily causes cracking and peeling of the polymer coating edges, exposing the steel substrate to the environment. After tape peeling, the pure organosilicon polymer coating peeled off over a large area. According to the test standards, its adhesion was rated at level 1A, indicating that the pure PA polymer exhibits poor adhesion under external force. With the addition of 5% PDMS, the area of coating peeling off significantly decreased. In samples at 5 days, 10 days, 20 days, and 30 days, there was almost no coating peeling off, and no pitting was observed at the edges. This indicates that PDMS reduces polymer shrinkage and enhances its durability. According to the standard, the adhesion of P-5 can reach the 5A level, which is the highest grade in the adhesion test standard. The polymer coating modified with 10% PDMS (P-10) also exhibited better adhesion (4A-5A) than the pure organosilicon polymer (P-0). When the PDMS content was increased to 15%, the modified polymer coating (P-15) peeled off in large areas after tape removal, similar to P-0. This is because the high PDMS content agglomerates and encapsulates unreacted fly ash and slag, affecting the initial depolymerization process, thereby impairing the formation of polymer gel and disrupting the cross-linking between the organic-inorganic network, resulting in reduced adhesion of the polymer to the steel plate surface.

4.2.2 | Viscosity strength

Figure 13 shows the bond strength of polymer steel sheet coatings with different PDMS content after curing for 3, 5, 10, 20, and 30 days.

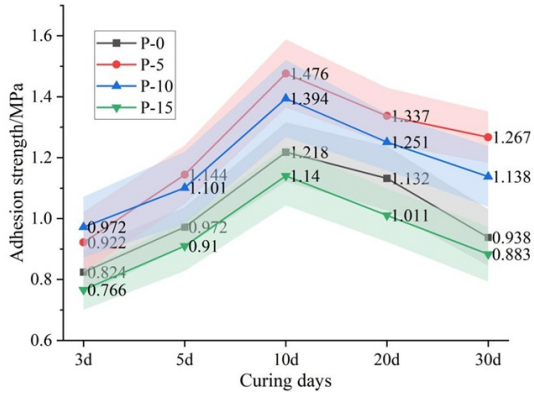

FIGURE 13 Bonding strength of geopolymer coatings with different PDMS dosages

The results indicate that after several days of curing, the bond strength between the modified polymer coating and the steel plate first increases and then decreases with increasing PDMS content, reaching a maximum at 5% PDMS content, consistent with the results of mechanical property testing. Compared to the pure polymer coating (P-0), the bond strength between the 5% PDMS-modified polymer coating (P-5) and the steel plate increased by 11.86%, 17.64%, 21.14%, 18.07%, and 35.08% after curing for 3 days, 5 days, 10 days, 20 days, and 30 days, respectively. As curing time increased, the bond strength between the pure organosilicon polymer coating and the PDMS-modified polymer coating and the steel plate both showed a trend of first increasing and then decreasing. After 30 days of curing, the bond strengths between the polymer coating and the modified polymer coating and the steel plate were 0.938 MPa, 1.267 MPa, 1.138 MPa, and 0.883 MPa, respectively, representing decreases of 23.03%, 14.17%, 18.38%, and 22.58% compared to the samples cured for 10 days. This is attributed to the formation of corrosion products. Since the steel plates were not coated around their edges, corrosive media could penetrate around the edges and form corrosion products on the steel plate surface, thereby affecting the bond strength. Among these, the pure organosilicon polymer coating showed the greatest decrease in bond strength, as pure organosilicon polymers exhibit significant drying shrinkage, leading to a substantial decline in performance after 30 days of curing. The bond strength between the modified polymers with 5% and 10% PDMS content and the steel plates remained within a relatively high range (1.1–1.3 MPa), indicating that the addition of PDMS effectively mitigates the drying shrinkage of the modified polymers. It can be inferred that the modified polymers enhance the density of the modified polymers, thereby more effectively preventing the intrusion of corrosive media and improving the corrosion resistance of the modified polymers.

4.2.3 | Open-circuit potential

This experiment only investigates the environmental simulation of two groups of PDMS-modified geopolymer steel sheet coatings (P-5, P-10) with relatively good comprehensive performance. Figures 14 and 15 show

the changes in open-circuit potential of PDMS-modified polymer samples in different simulated solutions over immersion time. In X-Y, X represents the PDMS content percentage, and Y represents the Cl-/OH- concentration ratio of the simulated solution; in C-X-Y, C represents the carbonization environment, and each point in the Figure is the average open-circuit potential of five identical samples.

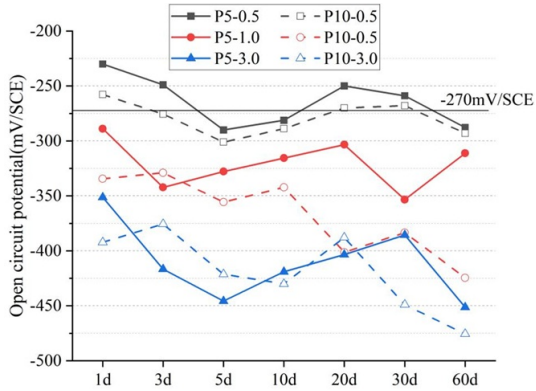

FIGURE 14 Evolution of modified coatings in Non-carbonized solutions

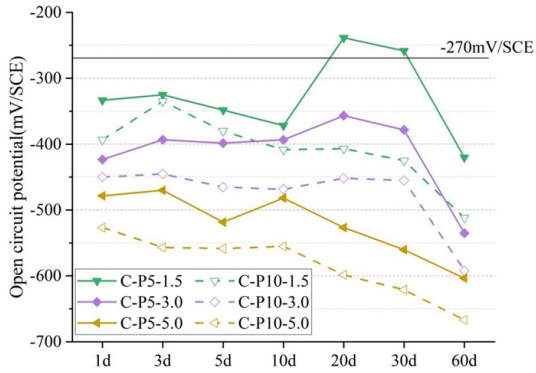

FIGURE 15 Evolution of modified coatings in carbonized solutions

Figure 14 shows that the corrosion potentials of the modified polymer coatings with 5% and 10% PDMS content in a non-carbonated solution are both at a relatively positive position. According to ASTM C876-09 standards, if the open-circuit potential of embedded reinforcing bars in concrete is below -270 mV/SCE, there is over a 90% likelihood of corrosion. In this experiment, bare steel plates were directly tested, so the open-circuit potential is relatively lower compared to the standard.

In samples with a Cl-/OH- concentration ratio of 0.5, the open-circuit potential of the modified polymer coating reached a steady state after 20 days of immersion (P-5: -250.25 mV/SCE, P-10: -268.61 mV/SCE), indicating that the modified polymer samples exhibit excellent corrosion resistance in low chloride ion environments. In a low chloride ion environment, the more compact structure of the polymer has sufficient capacity to prevent chloride ion penetration. At a Cl-/OH- concentration ratio of 1.0, after 30 days of immersion,

the corrosion potential of the modified polymer coating began to shift negatively, indicating that electrolytes gradually penetrated through the pores in the modified polymer coating, suggesting an increased likelihood of corrosion. Compared to samples in low chloride ion concentrations, the corrosion potential increases more significantly after 30 days when the Cl-/OH- concentration ratio is 3.0, suggesting that the modified polymer coating may also corrode after being immersed in a high chloride ion environment for an extended period. Under the same solution conditions, all geopolymer coatings with a 5% PDMS content exhibit a more positive corrosion potential than those with a 10% PDMS content, indicating that the 5% PDMS-modified geopolymer coating possesses superior corrosion resistance. This is attributed to the deeper cross-linking between the 5% PDMS and the polymer matrix network, forming more hydrotalcite-like phases and polymer gels, effectively reducing the penetration of the corrosive medium.

Figure 15 shows the trend of open-circuit potential changes in modified polymer coatings under carbonization conditions in simulated solutions with different Cl-/OH- ratios. Under the same chloride ion concentration as 1.0, the corrosion potential of the carbonized modified polymer coating tends to shift negatively. Compared with the two PDMS concentrations without carbonization, the corrosion potential of the carbonized coating is lower. This may be because the carbonates in the hydrotalcite phase occupy the interlayer hydroxyl positions of exchangeable chloride ions, reducing the interlayer exchange and surface adsorption capacity of the hydrotalcite phase. However, under the same chloride ion concentration, the reduction in OH- ions led to a significant decrease in the corrosion potentials of C-5-5.0 and C-10-5.0. This is because the absorption of chloride ions by the hydrotalcite-like phase is highly sensitive to changes in solution pH, chloride ion concentration, and total ionic strength. In the presence of carbonates in the pore solution, as the system's alkalinity decreases, the absorption of chloride ions by the hydrotalcite-like phase is significantly reduced, leading to a decline in the corrosion resistance of the modified polymer coating.

The prepared PDMS-modified geopolymer coatings exhibit relatively stable corrosion protection in low-chloride environments. Under high chloride ion concentration and carbonation conditions, modified geopolymer coatings with different PDMS content ratios maintain stable corrosion potentials within 30 days, but corrosion may occur after 30 days. Most importantly, the modified geopolymer coating with 5% PDMS content exhibits superior long-term corrosion protection performance.

4.2.4 | Polarization curve

To further investigate the influence of PDMS-modified polymer coatings on the corrosion resistance of steel plates in different solutions, polarization curves were characterized. Corrosion potential is a key parameter for assessing corrosion resistance; generally, the more positive the corrosion potential, the lower the probability of steel plate corrosion.

Immersion times of 5 days and 30 days were selected as the study subjects. Figures 16–19 show the polarization curves of the modified polymer coatings immersed in different solutions for varying durations.

Figures 16 and 17 show the polarization curves after 5 days of immersion in non-carbonated and carbonated solutions, respectively. It can be observed that as the immersion time increases, the corrosion potential of all modified polymer coatings decreases to varying degrees. Among them, the changes in the modified polymer coatings in non-carbonated environments are relatively small, indicating that the three-dimensional network structure of the geopolymer and the generated hydrotalcite-like phase have sufficient ability to hinder the penetration of chloride ions. The decrease in corrosion potential for the carbonized C-P5-5.0 and C-P10-5.0 coatings is more pronounced, suggesting that carbonate ions have become interlayer ions within the

hydrotalcite-like phase. The absorption of chloride ions by the hydrotalcite-like phase is highly sensitive to changes in solution pH, chloride ion concentration, and total ionic strength. In the presence of carbonate ions in the pore solution, a decrease in system alkalinity significantly reduces the absorption of chloride ions by the hydrotalcite-like phase; In contrast, C-P5-1.5 and C-P10-1.5 still maintain relatively positive corrosion potentials, which may be due to the presence of a larger amount of OH^- in the solution, which may delay the intrusion of chloride ions through concentration gradients.

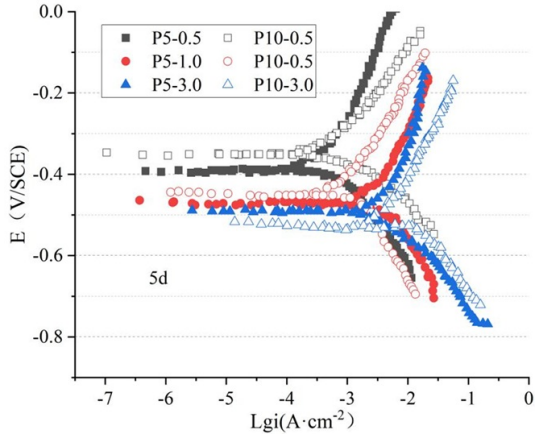

FIGURE 16 The TP curve of the coating immersed in non-carbonizing solution for 5d

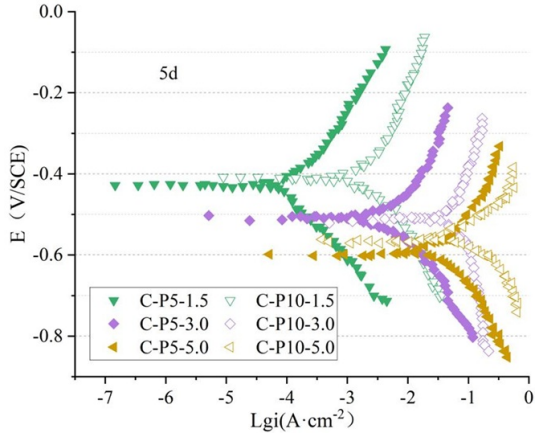

FIGURE 17 The TP curve of the coating immersed in carbonizing solution for 5d

As the immersion time reached 30 days, the polarization curves are shown in Figures 18 and 19. Except for a slight increase in the corrosion potential of P5-0.5, the corrosion potentials of all modified polymer coatings further decreased. Among them, the 5% PDMS-modified polymer coating exhibited a more positive corrosion potential and a smaller current density, indicating a lower risk of corrosion. It was also observed that the modified polymer coatings exhibited a decrease in corrosion current density even without carbonization,

suggesting that carbonization leads to a decline in the corrosion resistance performance of the modified polymer coatings.

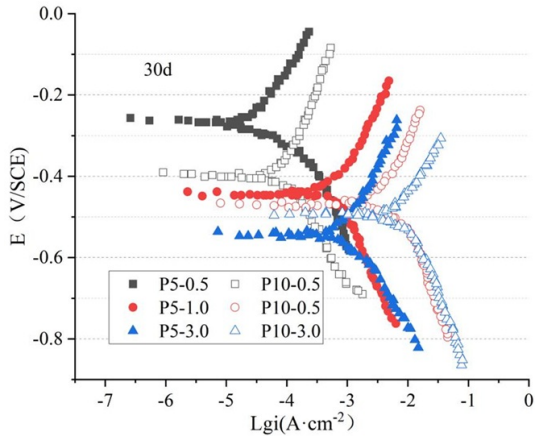

FIGURE 18 The TP curve of the coating immersed in non-carbonizing solution for 30d

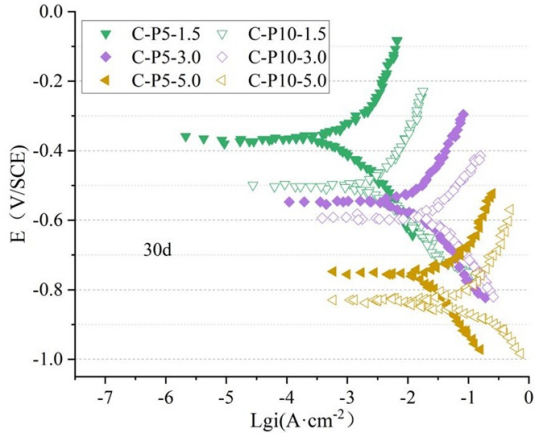

FIGURE 19 The TP curve of the coating immersed in carbonizing solution for 30d

5 | Conclusion

This study successfully synthesized organosilicon-modified water-based polyurethane (SiPU) and its composite resin (PDMS-g-PA) coating, and systematically evaluated their long-term corrosion resistance under simulated marine climate conditions.

FT-IR confirmed that PDMS was successfully incorporated into the polyurethane chain via Si-O-Si bonds (1010 cm^{-1}), and the characteristic -NCO peak (2400–2000 cm^{-1}) disappeared. The initial decomposition

temperature of SiPU reached 331°C, an increase of 91°C compared to unmodified PU (240°C); the glass transition temperature (Tg) decreased to -32.8°C (PU: -30.4°C), significantly improving the coating's high and low-temperature resistance.

Electrochemical impedance (EIS) testing showed that after 35 days of immersion in 0.1 mol/L HCl, the impedance arc radius of the 10% PDMS-g-PA coating expanded by >40% compared to the pure PA coating, confirming that PDMS enhances the barrier effect.

Long-term open-circuit potential (OCP) monitoring shows that the 5% PDMS-modified coating (P-5) maintains a stable OCP of -250.25 mV/SCE in a low-chloride environment (Cl-/OH- = 0.5), exceeding the corrosion risk threshold (-270 mV/SCE); In a high-chloride environment (Cl-/OH- = 3.0), the P-5 coating exhibited an OCP shift of <5% over 30 days, while the pure PA coating shifted by >15%.

Tape peel tests showed that the P-5 coating achieved the highest adhesion grade (5A), while the 15% PDMS coating (P-15) had its adhesion reduced to 1A–2A due to PDMS agglomeration. After 30 days of curing, the bond strength between the P-5 coating and the steel plate was 1.267 MPa, a 35.08% increase compared to the unmodified coating (0.938 MPa); while the bond strength of the P-15 coating decreased to 0.883 MPa.

Polarization curve analysis indicated that under carbonization conditions, the corrosion current density of the P-5 coating after 30 days was 18.7% lower than that of the P-10 coating, confirming its superior long-term protective capability. When the PDMS content exceeds 10%, organic-inorganic cross-linking is disrupted by silicone aggregation, leading to reduced adhesion; in a carbonization environment, competitive occupation of interlayer sites in the hydrotalcite phase weakens the coating's chloride ion blocking ability, causing the OCP to shift negatively by >20 mV.

The organosilicon-modified water-based coating (SiPU/PDMS-g-PA) with a 5% PDMS content exhibits the best performance in terms of adhesion (5 A), bond strength (1.267 MPa), thermal stability (decomposition at 331°C), and long-term corrosion resistance (OCP > -270 mV/SCE maintained for 60 days), providing a data-supported solution for metal protection in marine environments.

References

[1] Tavakoli, S., Khojasteh, D., Haghani, M., & Hirdaris, S. (2023). A review on the progress and research directions of ocean engineering. *Ocean Engineering, 272*, 113617.

[2] Song, S. Y., Guo, J., Su, Q. K., & Liu, G. (2020). Technical challenges in the construction of bridge-tunnel sea-crossing projects in China. *Journal of Zhejiang University-Science A, 21*(7), 509-513.

[3] Mainwaring, G., & Olsen, T. O. (2018). Long Undersea Tunnels: Recognizing and overcoming the logistics of operation and construction. *Engineering, 4*(2), 249-253.

[4] Aziz, A., Ahmed, S., Khan, F., Stack, C., & Lind, A. (2019). Operational risk assessment model for marine vessels. *Reliability Engineering & System Safety, 185*, 348-361.

[5] Raghukumar, S. (2017). Extreme marine environments. In *Fungi in Coastal and Oceanic Marine Ecosystems: Marine Fungi* (pp. 219-263). Cham: Springer International Publishing.

[6] Wu, S., Wu, S., Xing, S., Wang, T., Hou, J., Zhao, Y., & Li, W. (2024). Research progress of marine anti-fouling coatings. *Coatings, 14*(9), 1227.

[7] Jia, J., Cheng, X., Yang, X., Li, X., & Li, W. (2020). A study for corrosion behavior of a new-type weathering steel used in harsh marine environment. *Construction and Building Materials, 259*, 119760.

[8] Melchers, R. E., Jeffrey, R., Chaves, I. A., & Petersen, R. B. (2025). Predicting corrosion for life estimation of ocean and coastal steel infrastructure. *Materials and Corrosion, 76*(6), 776-789.

[9] Zhang, L., Niu, D., Wen, B., Peng, G., & Sun, Z. (2020). Corrosion behavior of low alloy steel bars containing Cr and Al in coral concrete for ocean construction. *Construction and Building Materials, 258*, 119564.

[10] Chung, S., Chen, Y., & Yang, C. (2018). Simulation of ocean environmental corrosion and analysis of visual communication effect. *Journal of Coastal Research, 83*, 603-608.

[11] Lee, H. S., Singh, J. K., & Ismail, M. A. (2017). An effective and novel pore sealing agent to enhance the corrosion resistance performance of Al coating in artificial ocean water. *Scientific Reports, 7*(1), 41935.

[12] Cao, H., Wang, K., Song, S., Zhang, X., Gao, Q., & Liu, Y. (2022). Corrosion behavior research and corrosion prediction of structural steel in marine engineering. *Anti-Corrosion Methods and Materials, 69*(6), 636-650.

[13] Kurth, J. C., Krauss, P. D., & Foster, S. W. (2019). Corrosion management of maritime infrastructure. *Transportation Research Record, 2673*(12), 2-14.

[14] Refait, P., Grolleau, A. M., Jeannin, M., Rémazeilles, C., & Sabot, R. (2020). Corrosion of carbon steel in marine environments: role of the corrosion product layer. *Corrosion and Materials Degradation, 1*(1), 10.

[15] Vigneron, A., Head, I. M., & Tsesmetzis, N. (2018). Damage to offshore production facilities by corrosive microbial biofilms. *Applied Microbiology and Biotechnology, 102*(6), 2525-2533.

[16] Procópio, L. (2019). The role of biofilms in the corrosion of steel in marine environments. World Journal of Microbiology and Biotechnology, 35(5), 73.

[17] Yan, L., Deng, W., Wang, N., Xue, X., Hua, J., & Chen, Z. (2022). Anti-corrosion reinforcements using coating technologies—A review. *Polymers, 14*(21), 4782.

[18] Dalmora, G. P. V., Borges Filho, E. P., Conterato, A. A. M., Roso, W. S., Pereira, C. E., & Dettmer, A. (2025). Methods of corrosion prevention for steel in marine environments: a review. *Results in Surfaces and Interfaces*, 100430.

[19] Zhang, H., Kong, F., Chen, Y., Zhao, X., Tang, Y., & Zuo, Y. (2023). Degradation of two anti-corrosion and anti-fouling coating systems in simulated diurnal cycling immersion. *Coatings, 13*(2), 389.

[20] Liu, S., Ma, L., Wang, J., Li, Y., Gong, H., Ren, H., ... & Zhang, D. (2025). Towards understanding and prediction of corrosion degradation of organic coatings under tropical marine atmospheric environment via a data-driven approach. *International Journal of Minerals, Metallurgy and Materials, 32*(5), 1151-1161.

[21] Çetinkaya, H. F., Seyran, E., Çetinkaya, S., & Tüzün, B. (2025). Corrosion Protection Coatings in Industrial Materials: Methods and Innovations. In *Advancing Corrosion Control with Metal– Organic Frameworks: Beyond Rust* (pp. 133-162). American Chemical Society.

[22] Yang, K., Chen, J., Zheng, L., Zheng, B., Chen, Y., Chen, X., ... & Xu, Y. (2021). Urushiol titanium polymer-based composites coatings for anti-corrosion and antifouling in marine spray splash zones. *Journal of Applied Polymer Science, 138*(34), 50861.

[23] Xiong, Y., Liu, H., Xu, J., & Chen, H. (2025). Mechanical properties of offshore floating photovoltaic structural coating/carbon steel system in a marine environment. *Ocean Engineering, 323*, 120585.

[24] Zhang, B., Qiao, M., Xu, W., & Hou, B. (2022). All-organic superhydrophobic coating with anti-corrosion, anti-icing capabilities and prospective marine atmospheric salt-deliquesce self-coalesce protective mechanism. *Journal of Industrial and Engineering Chemistry, 115*, 430-439.

[25] Liu, Z., Zheng, X., Zhang, H., Li, W., Jiang, R., & Zhou, X. (2022). Review on formation of biofouling in the marine environment and functionalization of new marine antifouling coatings. *Journal of Materials Science, 57*(39), 18221-18242.

[26] Song, D., Qin, W., Zhou, Q., Xu, D., & Zhang, B. (2023). Correlation between the initial aging of epoxy coatings and the typical marine atmospheric environmental factors. *Anti-Corrosion Methods and Materials, 70*(6), 547-563.

[27] Maniam, K. K., & Paul, S. (2021). Corrosion performance of electrodeposited zinc and zinc-alloy coatings in marine environment. *Corrosion and Materials Degradation, 2*(2), 163-189.

[28] Wang, C., Wu, M., Wang, Y., Wang, J., Wen, Z., Wei, W., & Miao, X. (2023). Effect of Al2O3-MWCNTs on anti-corrosion behavior of inorganic phosphate coating in high-temperature marine environment. *Surface and Coatings Technology, 473*, 130039.

[29] Liang, H., Shi, X., & Li, Y. (2024). Technologies in marine antifouling and anti-corrosion coatings: a comprehensive review. *Coatings, 14*(12), 1487.

[30] Xue, X., Liang, G., & Zhang, B. (2025). Superhydrophobic anti-corrosion coating: Advancing research from laboratory to real marine corrosion environment. *Progress in Organic Coatings, 200*, 109020.

[31] Sabet-Bokati, K., Bakhshandeh, E., Russell, Z., Gaier, M., & Plucknett, K. P. (2025). Critical investigation of the long-term integrity of sustainable anti-corrosion coatings in static and dynamic humid environments. *Progress in Organic Coatings, 204*, 109276.

[32] Wang, Z., Zhou, Z., Xu, W., Yang, D., Xu, Y., Yang, L., ... & Huang, Y. (2021). Research status and development trends in the field of marine environment corrosion: a new perspective. *Environmental Science and Pollution Research, 28*(39), 54403-54428.

[33] Vera, R., Bagnara, M., Henríquez, R., Muñoz, L., Rojas, P., & Díaz-Gómez, A. (2023). Performance of anticorrosive paint systems for carbon steel in the antarctic marine environment. *Materials, 16*(16), 5713.

[34] Song, G. L., & Feng, Z. (2020). Modification, degradation and evaluation of a few organic coatings for some marine applications. *Corrosion and Materials Degradation, 1*(3), 408-442.

[35] Wu, X., Yang, C., Wu, L., Zhang, C., Cui, G., & Xin, Y. (2023). Self-repairing and anti-fouling performance of anticorrosive coating in marine environment. *Polymer Testing, 124*, 108090.

[36] Yu, M., Fan, C., Ge, F., Lu, Q., Wang, X., & Cui, Z. (2021). Anticorrosion behavior of organic offshore coating systems in UV, salt spray and low temperature alternation simulated Arctic offshore environment. *Materials Today Communications, 28*, 102545.

[37] Zhao, X., Chen, C., Xu, W., Zhu, Q., Ge, C., & Hou, B. (2017). Evaluation of long-term corrosion durability and self-healing ability of scratched coating systems on carbon steel in a marine environment. *Chinese Journal of Oceanology and Limnology, 35*(5), 1094-1107.

[38] Zhang, P., Zhao, Y., Gu, X., Yang, K., Zhang, X., Liu, M., ... & Che, Y. (2024). Constructing carbon nanotube (CNTs)/silica superhydrophobic coating with multi-stage rough structure for long-term anti-corrosion and low-temperature anti-icing in the marine environment. *Composites Science and Technology, 257*, 110798.

[39] Eom, S. H., Kim, S. S., & Lee, J. B. (2020). Assessment of anti-corrosion performances of coating systems for corrosion prevention of offshore wind power steel structures. *Coatings, 10*(10), 970.

[40] Wang, S., Liu, Q., Wang, J., Chen, N., Chen, J., Song, J., ... & Xiao, K. (2024). Study of the role of aluminium and corrosion mechanism in galvalume coating in the marine atmospheric environment. *Anti-Corrosion Methods and Materials, 71*(3), 286-294.